Original Paper

Cellular Physiology and Biochemistry

Cell Physiol Biochem 2012;29:761-774

Accepted: February 23, 2012

An Inhibitory Peptide Derived from the α-subunit of the Epithelial Sodium Channel (ENaC) Shows a Helical Conformation

Silke Haerteis[1], Daniel Schaal[2], Felix Brauer[2], Stefan Brüschke[2], Kristian Schweimer[2], Robert Rauh[1], Heinrich Sticht[4], Paul Rösch[2,3], Stephan Schwarzinger[2,3] and Christoph Korbmacher[1]

[1]Institut für Zelluläre und Molekulare Physiologie, Friedrich-Alexander-Universität Erlangen-Nürnberg, Erlangen, [2]Lehrstuhl Biopolymere, Universität Bayreuth, Bayreuth, [3]Research Center for Bio-Macromolecules, Universität Bayreuth, Bayreuth,[4]Abteilung für Bioinformatik, Institut für Biochemie, Friedrich-Alexander-Universität Erlangen-Nürnberg, Erlangen

Key Words
Ion channel • Sodium transport • *Xenopus laevis* oocytes • Electrophysiology • NMR • Peptides

Abstract
Proteolytic activation of the heteromeric epithelial sodium channel (ENaC) is thought to involve the release of inhibitory peptides from the extracellular domains of its α- and γ-subunit. Recently, we demonstrated that an α-13-mer peptide, corresponding to a putative inhibitory region within the extracellular domain of human αENaC, inhibits human αβγENaC. The aim of the present study was to investigate the structural basis of the inhibitory effect of this α-13-mer peptide. Analysis of the peptide by replica exchange molecular dynamics method, circular dichroism spectroscopy, nuclear magnetic resonance spectroscopy, and molecular dynamics simulations suggested that a helical turn at the carboxy-terminus is the preferred conformational state of the α-13-mer peptide. From this we predicted that a specific mutation (leucine 188 to alanine) should have a strong effect on the conformational preferences of the peptide. To functionally test this, we compared the effect of the wild-type α-13-mer with that of a mutant α-L188A-13-mer on ENaC currents in *Xenopus laevis* oocytes heterologously expressing human αβγENaC. We demonstrated that replacing the leucine 188 by alanine abolished the inhibitory effect of the α-13-mer peptide on ENaC. These findings suggest that a helical conformation in its carboxy-terminal part is functionally important to mediate ENaC inhibition by the α-13-mer peptide. However, high resolution structural information on the complex of the inhibitory αENaC peptide and the channel are needed to confirm this conclusion.

Introduction

The amiloride-sensitive epithelial sodium channel (ENaC) is a member of the ENaC/degenerin family of non-voltage gated ion channels [1]. Typically, ENaC is localized in the apical membrane of polarized epithelial cells in sodium-absorbing epithelia

KARGER
Fax +41 61 306 12 34
E-Mail karger@karger.ch
www.karger.com

1015-8987/12/0296-0761$38.00/0

Accessible online at:
www.karger.com/cpb

Prof. Dr. med. C. Korbmacher, Institut für Zelluläre und Molekulare Physiologie, Friedrich-Alexander-Universität, Waldstr. 6, D-91054 Erlangen (Germany)
E-Mail christoph.korbmacher@physiologie2.med.uni-erlangen.de
and PD Dr. S. Schwarzinger, Lehrstuhl Biopolymere, Universität Bayreuth Bayreuth (Germany), E-Mail stephan.schwarzinger@uni-bayreuth.de

like the aldosterone-sensitive distal nephron (ASDN), respiratory epithelia, distal colon, sweat and salivary ducts. In these epithelia ENaC is the rate limiting step for transepithelial sodium absorption and has to be tightly regulated. ENaC regulation in the ASDN plays a critical role in the maintenance of body sodium balance and the long-term control of arterial blood pressure [2, 3]. In epithelial tissues ENaC is composed of three homologous subunits (α, β, γ). Each subunit contains two transmembrane domains (M1 and M2), a large extracellular domain, and short intracellular amino and carboxyl-termini. The published crystal structure of the related acid-sensing ion channel (ASIC1) [4-6] and recent atomic force microscopy data of ENaC [7] suggest that ENaC is a heterotrimer.

Proteolytic processing of ENaC along its biosynthetic pathway and at the cell surface is believed to be an important mechanism for channel activation [8, 9]. The channel is thought to be in its mature and active form in its fully cleaved state, but there is evidence for the presence of both cleaved and non-cleaved channels in the plasma membrane [10]. Cleavage occurs at specific sites within the extracellular domains of the α- and γ-subunits but not the β-subunit. Cleavage at these sites probably causes a conformational change of the channel by the release of inhibitory peptides from the extracellular domains of α- and γENaC [11-14].

The concept that peptide sequences with an inhibitory effect on ENaC are released is supported by the finding that synthetic peptides with an amino acid sequence corresponding to the predicted cleavage products inhibit ENaC activity *in vitro*. Indeed, a synthetic 26- or 43-mer peptide corresponding to excised fragments of α- or γENaC, respectively, has been shown to inhibit mouse αβγENaC expressed in *Xenopus laevis* (*X. laevis*) oocytes and endogenous ENaC in cultured mouse collecting duct epithelial cells [11, 12]. An 8-mer peptide (α-8-mer) corresponding to an eight-residue amino acid tract within the previously described inhibitory α-26-mer appears to be critical for mediating this inhibitory effect [13]. Similarly, systematic analysis of the excised fragment from the γ-subunit indicated that an eleven-residue amino acid tract is essential for channel inhibition [14].

So far, our knowledge on the proteolytic activation of ENaC is mainly based on studies using ENaC from mouse or rat. However, the process of proteolytic channel activation appears to be similar for human ENaC [15-17]. Recently, we investigated the effect of a synthetic 13-mer peptide (α-13-mer) corresponding to amino acid residues 180-LRGTLPHPLQRLR-192 in the extracellular domain of human αENaC [16]. This region shows a high degree of identity to the inhibitory region identified in mouse αENaC and includes the eight amino acid residues of the inhibitory mouse α-8-mer peptide (211-LPHPLQRL-218) in identical sequence [13]. We demonstrated that this α-13-mer inhibits human αβγENaC expressed in *X. laevis* oocytes consistent with the inhibitory effect of the α-8-mer peptide on mouse ENaC [16].

At present it is unclear, how the inhibitory α- or γ-peptides added to the channel can cause an inhibition of ENaC activity. The finding that the α-13-mer peptide inhibits αβγ- but not δβγENaC indicates that the α-subunit is necessary for the inhibitory action of the peptide [16]. Moreover, there is evidence that the α-8-mer peptide is an allosteric inhibitor of ENaC stabilizing its closed state [18]. The inhibitory ENaC peptides are thought to bind to specific regions of the channel thereby inducing a conformational change that favors the closure of the channel. In non-cleaved channels the three-dimensional arrangement of the extracellular domain may allow the inhibitory peptide region to bind to an inhibitory site or binding pocket. Cleavage of the inhibitory peptide region may terminate tonic channel inhibition by the inhibitory region thereby leading to channel activation. The finding that both, inhibitory α- and γ-peptides, can inhibit ENaC activity is consistent with the concept that only fully cleaved channels are active. Thus, adding back one of the cleaved inhibitory peptides is expected to be sufficient for channel inhibition. A recent modeling approach [19] was based on functional data of mutations that attenuate inhibitory peptide binding in combination with comparative modeling using the reported crystal structure of ASIC1 [5]. This modeling predicts that the α-8-mer inhibitory peptide affects channel gating by constraining motions within two major domains in the extracellular region of the channel, the so called thumb and finger domains. However, the precise location and nature of the putative binding pockets for the inhibitory peptides remain to be determined.

This leads to the interesting question whether an analysis of the molecular structure of the inhibitory α-peptide can help to provide some insight into how it may interact with a putative binding pocket to affect channel function. Therefore, the aim of the present study was to investigate the structural basis of the inhibitory effect of the human α-13-mer peptide on ENaC. To obtain information about the preferred conformational state of

the human α-13-mer peptide, we used the replica exchange molecular dynamics method (REMD), circular dichroism (CD) spectroscopy, nuclear magnetic resonance (NMR) spectroscopy, and molecular dynamics (MD) simulations. From our structural model of the α-13-mer peptide we predicted that a specific mutation (leucine 188 to alanine) should have a strong effect on its conformational preferences. In functional studies using the *X. laevis* oocyte expression system and the two-electrode voltage-clamp technique we compared the inhibitory effects of the wild-type (wt) α-13-mer and the mutant α-L188A-13-mer on heterologously expressed human αβγENaC.

Materials and Methods

Plasmids

Full-length cDNAs for human α-, β- and γENaC were kindly provided by Harry Cuppens (Leuven, Belgium). They were subcloned into pcDNA3.1 vector, and linearised plasmids were used as templates for cRNA synthesis (mMessage mMachine, Ambion, Austin, Texas, USA) using T7 as promotor.

Isolation of Oocytes and Injection of cRNA

Adult female *X. laevis* were anaesthetized in 0.2 % MS222 (Sigma Aldrich, Taufkirchen, Germany) to perform partial ovariectomy. Oocytes were isolated from the ovarian lobes by enzymatic digestion with 600-700 U/ml collagenase CLS 2 (Biochrom, Berlin, Germany) dissolved in OR2 solution at 19°C for 3-4 h on a tumbling table. Defolliculated stage V-VI oocytes were injected with an equal amount of cRNA per ENaC subunit (0.5-1 ng per subunit). The cRNAs were dissolved in RNase-free water and the total volume injected into each oocyte was 46 nl. Injected oocytes were stored at 19°C in ND9 (low Na^+) solution. To prevent bacterial overgrowth the solutions were supplemented with 100 U/ml sodium penicillin and 100 µg/ml streptomycin sulphate.

Two-Electrode Voltage-Clamp (TEVC)

Oocytes were routinely studied two days after injection using TEVC essentially as described previously [16, 20]. The oocytes were placed in a small experimental chamber and constantly superfused with ND96 at a rate of 2-3 ml/min at room temperature. For continuous whole-cell current recordings oocytes were routinely clamped at a holding potential of -60 mV. Negative currents are per definition inwardly directed and represent either movement of positive charge into the cell or movement of negative charge out of the cell. Amiloride-sensitive whole-cell currents (ΔI_{ami}) were obtained by washing out amiloride (2 µM) with amiloride-free ND96 and subtracting the whole-cell currents measured in the presence of amiloride from the corresponding whole-cell currents recorded in the absence of amiloride.

Solution and Chemicals

Amiloride hydrochloride was purchased from Sigma and was added to the bath solution from an aqueous 10 mM stock solution. OR2 solution for the oocyte preparation contained in mM: NaCl 82.5, KCl 2, $MgCl_2$ 1, HEPES 5 (pH 7.4 with NaOH). ND9 solution for the oocyte incubation: NaCl 9, NMDG-Cl 87, KCl 2, $CaCl_2$ 1.8, $MgCl_2$ 1, HEPES 5. ND96 solution for the electrophysiological measurements: NaCl 96, KCl 2, $CaCl_2$ 1.8, $MgCl_2$ 1, HEPES 5. In these two solutions the pH was adjusted to pH 7.4 with Tris.

Peptides

The wt α-13-mer peptide (sequence: LRGTLPHP**L**QRLR) as well as the mutant α-L188A-13-mer peptide (sequence: LRGTLPHP**A**QRLR) were synthesized and purified by high performance liquid chromatography (purity > 95%) by Coring System Diagnostix GmbH (Gernsheim, Germany). The peptides were modified by amino-terminal acetylation and carboxy-terminal amidation to prevent unwanted charge effects of the end groups. They were dissolved in ND96 stock solution at a concentration of 27 µM. Aliquots of this stock solution were kept at -80°C and were added to the bath solution on the day of the experiment in concentrations as indicated.

Replica Exchange Molecular Dynamics (REMD)

REMD was carried out with the AMBER10 [21] software package on a dual-quadcore computing node using the ff99SB force field and a generalized born environment (igb 5) to simulate the solvent utilizing the *mbondi2* atom radii. The wt α-13-mer peptide was initially minimized. Subsequently, eight replicas were simulated at temperatures of 269.5 K, 300 K, 334 K, 371.8 K, 413.9 K, 460.7 K, 512.9 K, and 570.9 K (http://ambermd.org/tutorials/advanced/tutorial7), respectively, which resulted in sufficient exchange between the individual replicas. To prevent unwanted conformational changes in the peptide bonds at high temperatures, corresponding chirality restraints were placed using the DISANG function during equilibration and production runs. Equilibration (100 ps per replica) and replica exchange were carried out using a 2 fs time step in multi-SANDER [21]. In total, per replica 250.000 exchange attempts were tried every 25 time steps, resulting in a total simulation time of 100 ns for all replicas (12.5 ns per replica). Energy data were stored every 0.2 ps, structures every 2 ps. Trajectories were analyzed for preferred conformations by grouping into ten clusters of structures utilizing the hierarchical cluster algorithm from AMBER's PTRAJ tool employing the rms as distance metric [21].

Circular Dichroism (CD) Spectroscopy

CD spectra were measured on a JASCO J-810 spectro-polarimeter equipped with a CDF-426S Peltier element for temperature control. Lyophilized wt α-13-mer and α-L188A-13-mer were dissolved in 10 mM potassium phosphate buffer at pH 7. For measurements with trifluorethanol (TFE) this was added to a final concentration of 15 or 30 % (v/v). Spectra were collected in a 0.1 cm quartz

cell from 260 nm to 180 nm using the step mode with a step size of 0.2 nm, an integration time of 2 s, the sensitivity set to 100 mdeg, and the temperature set to 293 K. An additional measurement was made at 278 K to demonstrate essentially identical behavior at the lower temperature used for NMR. Peptide concentrations of the solutions were determined to 50 µM and 39 µM for the wt α-13-mer and the mutant α-L188A-13-mer, respectively, by absorption measurements at 205 nm and 210 nm [22, 23]. Spectra were baseline corrected by subtracting spectra of the pure buffer or the buffer with TFE and smoothed with a Savitzky-Golay algorithm using a window size of 11. Helical contents were estimated at 222 nm according to the method of Chen et al. [24].

Nuclear Magnetic Resonance (NMR) Spectroscopy and Structure Calculation

Samples for NMR-spectroscopy were prepared by dissolving lyophilized peptides in 10 mM potassium phosphate, pH 7, with either 10 % D_2O or 30 % deuterated TFE-d3 as lock substance and with 100 µM DSS (2,2-dimethyl-2-silapentane-5-sulfonic acid) as internal standard. Spectra were recorded on Bruker Avance-NMR spectrometers operating at 800 MHz equipped with a TCI-cryogenic probe with z-axis gradients and 600 MHz equipped with a TXI probe with z-axis gradients. ^{1}H-1D spectra were typically recorded using a W5-sequence for water suppression. Initial spectra were collected at various temperatures in a range between 298 K to 268 K. Subsequent standard two-dimensional through-bond (TOCSY (total correlation spectroscopy), DQF-COSY (double-quantum-filtered spectroscopy) and through-space proton correlation experiments (NOESY; nuclear Overhauser enhancement spectroscopy)) were recorded at 278 K for resonance assignment and derivation of structure defining NMR parameters [25]. Spectra were processed using NMRPipe [26] and analyzed with NMRView or NMRViewJ, respectively [27]. Sequential assignment was achieved by using TOCSY, NOESY and DQF-COSY spectra. Secondary structure propensities were estimated using the H^N and H^α chemical shift indices [28-30]. For determination of preferred peptide conformers NOESY signals were picked in spectra with mixing times with 100 ms and with 300 ms, respectively, and subjected to structure calculation using XPLOR-NIH [31-33]. NOE-cross peak volumes were converted into distance constraints by calibration against the intra-residual H^N-H^α cross peak set to 0.3 nm. To evaluate the influence of the force-field control calculations were conducted without experimental restraints. Structures were evaluated using PROCHECK [34]. RMSD values were calculated using VMD [35].

Molecular Dynamics (MD)

MD simulations were carried out using the AMBER10 suite of programs and the ff99SB force field to evaluate differences in the conformational dynamics between the wt and the L188A mutant of the ENaC-13-mer peptide [21, 36]. The lowest energy structures from the NMR-ensemble of α-13-mer and α-L188A-13-mer were selected as starting structures, respectively. Peptides were solvated by a 10 Å water sphere (approx. 4000 TIP3P water molecules), relaxed, heated to 300 K, and equilibrated using a 2 fs time step in combination with the SHAKE option under constant volume. Production runs were performed for a total of 6 ns under constant pressure for the wt peptide as well as the mutant peptide (http://ambermd.org/tutorials/basic/tutorial1/). Data were analyzed with respect to secondary structure contents using the PTRAJ tool of AMBER10.

Statistical Methods

Data are presented as mean ± SEM and were analyzed using GraphPad Prism 4.01 for Windows (Graph Pad Software Inc., San Diego, California, USA). Statistical significance was assessed by appropriate version of Student's t-test. *N* indicates the number of different batches of oocytes, *n* the number of individual oocytes studied.

Results

The synthetic human α-13-mer peptide shows a concentration-dependent inhibitory effect on human ENaC

In an initial set of experiments we confirmed the inhibitory effect of the α-13-mer on human αβγENaC and investigated the concentration dependence of its effect. A typical whole-cell current recording from a human αβγENaC expressing oocyte at a continuous holding potential of -60 mV is shown in Fig. 1A. In the presence of the specific ENaC inhibitor amiloride (2 µM) in the bath solution the inward current was minimal. Washout of amiloride resulted in an initial transient inward current component followed by a rapid decay to a sustained inward current plateau. The rapid current decay represents Na^+ self inhibition which is a well-known characteristic of ENaC [20, 37, 38]. After the current had reached a plateau the successive application of increasing concentrations (0.027 µM; 0.27 µM; 0.85 µM; 2.7 µM; 27 µM) of the human α-13-mer demonstrated a concentration-dependent inhibitory effect of the peptide on the ENaC-mediated inward current. Amiloride (2 µM) applied in the presence of the highest concentration of the peptide (27 µM) had an additional inhibitory effect indicating that ENaC inhibition by the peptide is incomplete. Time matched control experiments with mock solution exchanges (Fig. 1B) demonstrated that the inhibitory effect of the α-13-mer peptide cannot be attributed to spontaneous channel run-down known to occur in oocytes heterologously expressing ENaC [39]. As summarized in Fig. 1C the α-13-mer peptide has a concentration-dependent inhibitory

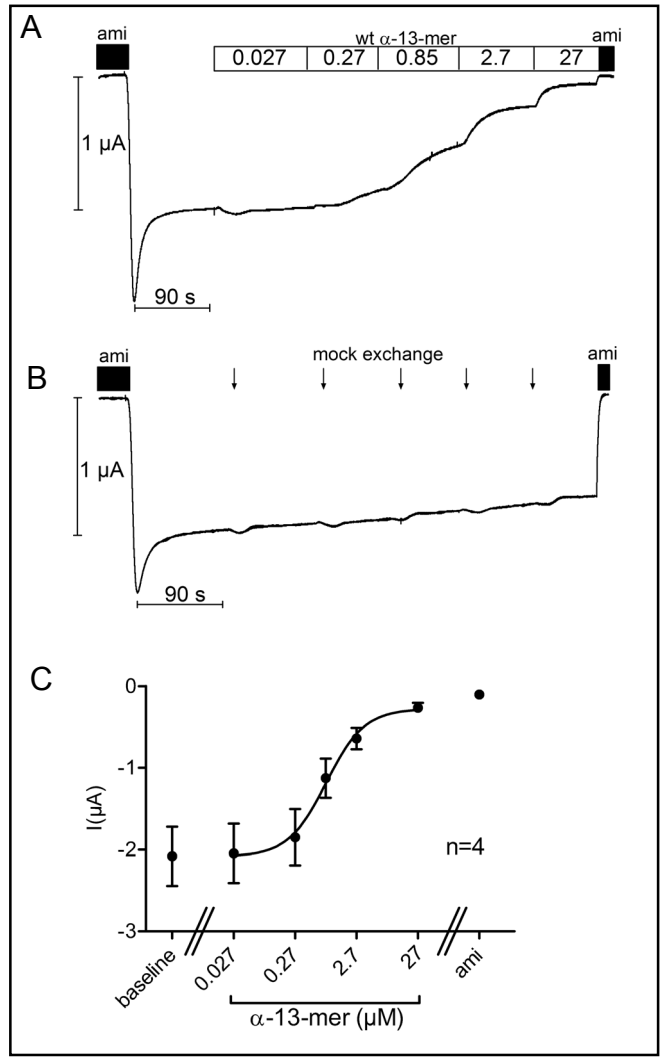

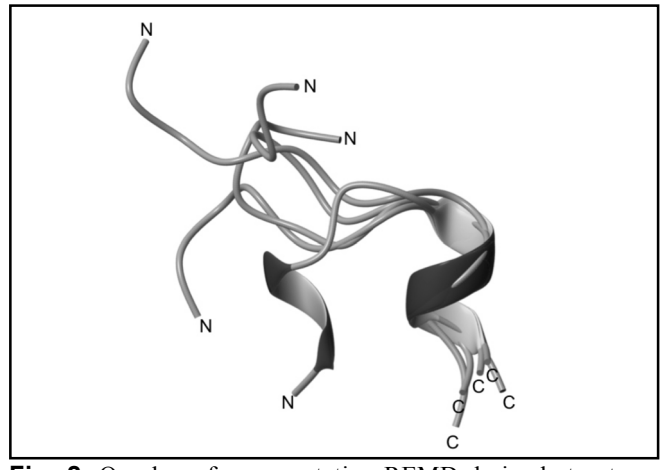

Fig. 1. Whole-cell currents were recorded from human αβγENaC expressing *X. laevis* oocytes clamped at a continuous holding potential of -60 mV. A: Representative current trace from an experiment in which increasing concentrations (in µM) of the α-13-mer peptide were applied as indicated by the open bars. Amiloride (2 µM) was present as indicated by the filled bars. B: Control recording with mock solution exchanges at the time points indicated by arrows. C: Average concentration-response curve estimated from experiments as shown in *A*. The value prior to the application of the peptide is indicated with 'baseline'.

effect on human ENaC currents with an estimated IC_{50} of 0.86 µM. This value is in excellent agreement with the IC_{50} of 0.9 µM reported for the inhibitory effect of the mouse α-8-mer peptide on mouse ENaC expressed in *X. laevis* oocytes [13].

1D-NMR spectra and REMD indicate the presence of preferred conformations in the inhibitory peptide

Initial 1D-NMR spectra of the wt α-13-mer in aqueous buffer at 298 K exhibited some unexpected broad line intensities for this rather small peptide changing with varying temperature. Spectra of a 10-times diluted sample indicated identical line widths (data not shown). Therefore, the existence of broad lines was attributed to exchange between different conformations in the conformational ensemble on the intermediate chemical shift timescale (µs to ms). To explore the conformational space, REMD simulations were conducted with the wt α-13-mer. Cluster analysis of the eight replicas by structural similarity revealed a preference for α-helical conformations in the carboxy-terminal region of the peptide, which includes the minimal eight amino acid inhibitory sequence [13]. In contrast, the amino-terminal region exhibits no structural preferences (Fig. 2).

To test whether or not helical structures can be populated in the wt α-13-mer, CD spectra were collected with and without the helix-promoting agent TFE [40]. Although not physiological, TFE apparently can stabilize preferred conformations in the peptides under investigation. Importantly, TFE cannot induce helix formation in sequences that do not have an intrinsic preference to form helices as shown in studies of model peptides from the helical protein apo-myoglobin [41]. In the absence of TFE, the wt α-13-mer exhibits a pronounced minimum at 197 nm indicative for

Fig. 2. Overlay of representative REMD-derived structures from the five clusters with the highest populations, which together represent over 70 % of the clustered structures. Amino- and carboxy-termini are labeled by "N" or "C", respectively. The ensemble clearly shows formation of a helix in the region of the inhibitory sequence. Notably, also the remaining clusters exhibit helical conformations in the carboxy-terminus (data not shown).

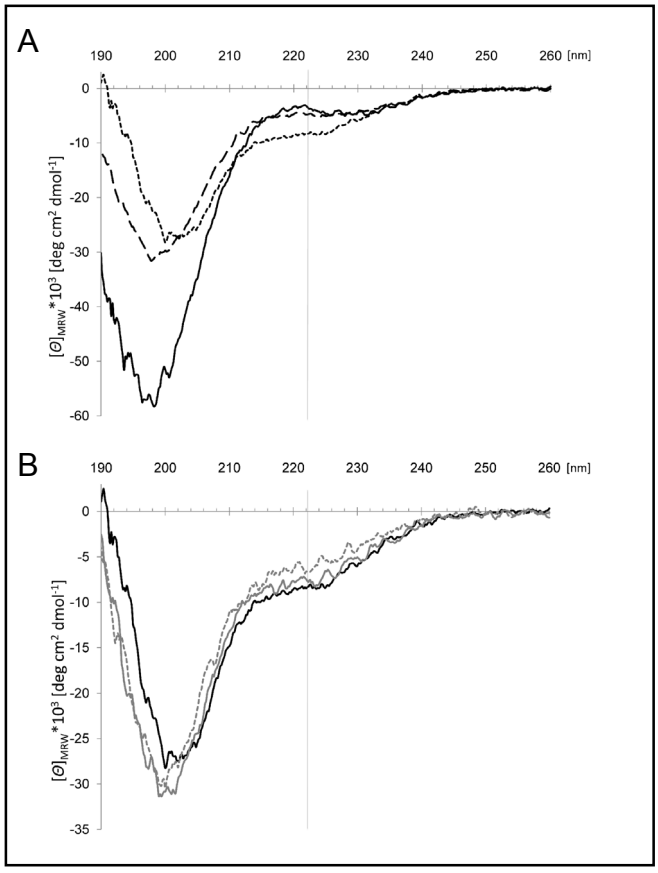

Fig. 3. CD spectra of inhibitory ENaC peptides. A: wt α-13-mer with increasing amounts of TFE at 293 K. A decrease of the CD-signal at 222 nm indicates an increase of helical structures with increasing TFE concentrations (0 % TFE: solid black line; 15 % TFE: broken line; 30 % TFE: dotted line). B: Comparison of the CD spectra of wt peptide (solid black line) and the L188A variant (solid grey line) indicates a slightly reduced helix content of the mutant at 293 K (wt: 26 %, L188A: 23 %). At lower temperatures, as used for NMR-studies, the helix content decreases further to approximately 20 % for the L188A variant (dotted grey line). The vertical grey line at 222 nm indicates the wavelength used to estimate the helix content.

random conformations. Increasing amounts of TFE in the solution introduced a shift of this minimum towards longer wavelengths and a change in intensity at 222 nm indicating the presence of α-helical conformations (Fig. 3A). At 30 % TFE the helix content was estimated to be 26 %. Taken together, 1D-NMR spectra indicate conformational exchange on the NMR time scale in the wt α-13-mer, i.e. a change between different conformations typically on the μs to ms timescale that leads to broadening and eventually the loss of NMR signals. Furthermore, REMD simulations and CD-experiments with TFE point towards preferred conformations with increased content in α-helix.

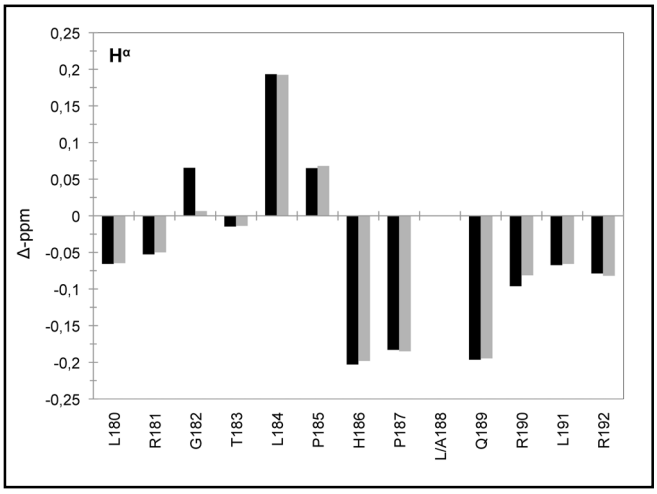

Fig. 4. Secondary chemical shifts (Δ-ppm) for H^{α} from the wt α-13-mer peptide (black bars) and the L188A mutant (grey bars). Δ-ppm values correspond to the difference of the observed chemical shifts and the chemical shifts on random coil reference peptides [28-30]. Negative values indicate the presence of helical structures, alternating signs are indicative of random structures. L188 and A188 have been omitted as these residues could not be assigned unambiguously or are even absent in the spectra presumably as a result of conformational exchange.

2D-NMR spectra of wt α-13-mer in TFE reveal helical conformations for the inhibitory sequence

We subsequently determined the preferred conformer in the ensemble of wt α-13-mer by homo-nuclear 2D-NMR spectroscopy in 30 % TFE. Except for L188 the backbone and β-protons of all residues could be assigned and were used for structure calculations. Signals for L188 appear to overlap with other signals or are absent which would be in line with the assumption of conformational exchange made above. Secondary structure propensities were estimated from the assigned H^{α} resonances by calculating the chemical shift difference to random coil reference shifts that were corrected for the influence of the local amino acid sequence [30]. Values with alternating signs as found in the amino-terminal portion of the sequence of wt α-13-mer are indicative of truly random conformational ensembles. In contrast, only negative values can be found between H186 and R192 indicating α-helix formation in this region (Fig. 4). These data are in line with the REMD simulations and the CD data and indicate that helical structures are indeed preferred for the sequence corresponding to the minimal eight amino acid inhibitory sequence. Consequently,

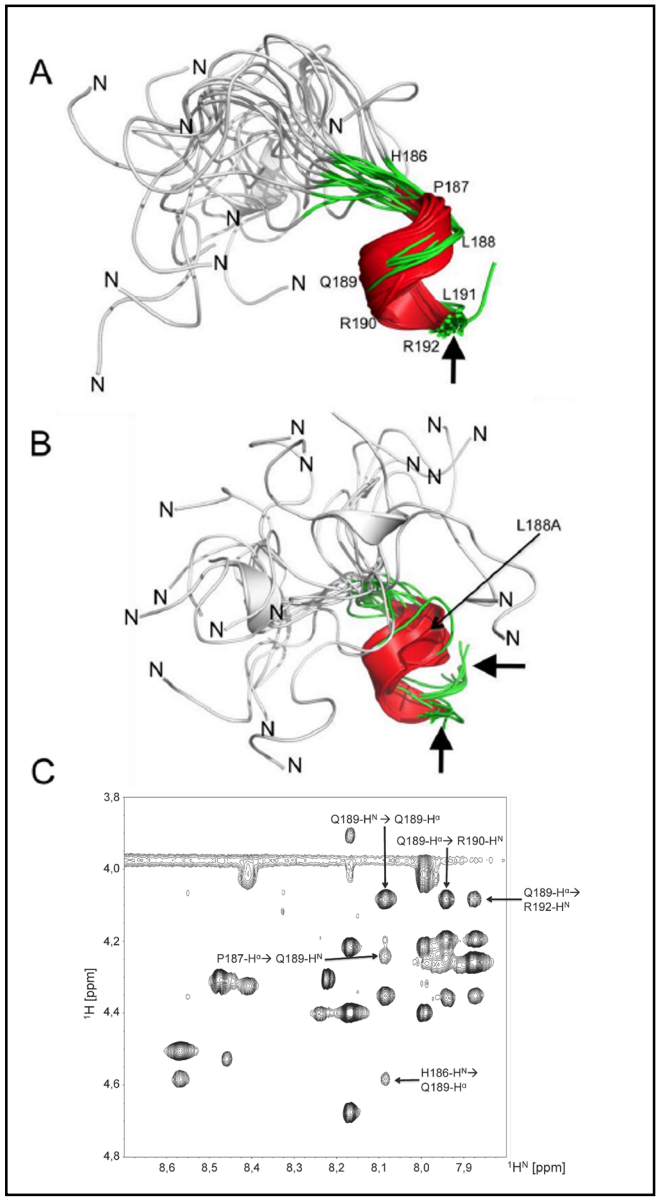

Fig. 5. NMR-derived structural ensembles containing the 20 lowest energy structures of the wt- (A) and the L188A variant (B) of the inhibitory α-13-mer peptide of the ENaC α-subunit. Amino-termini are labeled with an „N“, the helical carboxy-terminus is marked by a bold arrow. α-helices are colored red, disordered parts in the carboxy-terminal half are shown in green while the amino-terminal flexible part is depicted in grey (figures prepared with PyMol (Schrödinger LLC, USA)). Panel (C) depicts a section of the NOESY spectra (300 ms mixing time) of the wt α-13-mer peptide. Cross peaks between residues typical for helical conformers are marked by arrows. Of note, cross peak intensities as well as cross-peak patterns are in agreement with helical conformations in these cases.

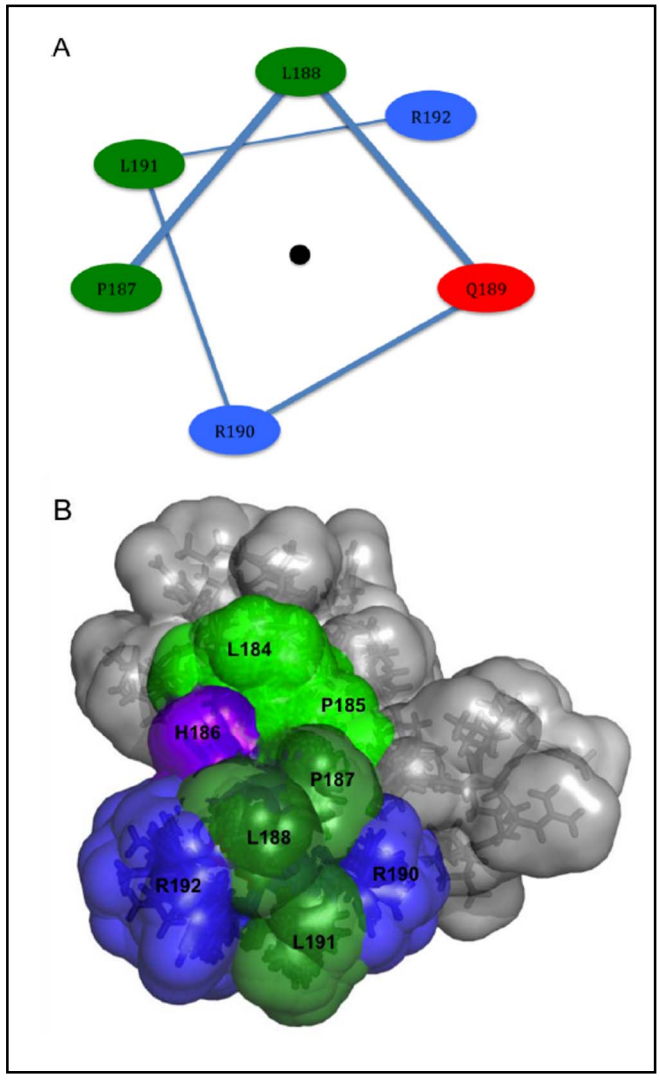

Fig. 6. Amphiphatic carboxy-terminal helix of wt α-13-mer peptide shows a hydrophobic and a hydrophilic side. A: Helical wheel plot of the carboxy-terminal half of the inhibitory active sequence including the capping proline at position 187. Amino acids are color-coded to reflect their polarity (green: apolar; blue: positive potential; red: negative potential; the central black dot symbolized the helical axis). The clear separation into a hydrophobic and a polar half of this single helix turn is immediately visible. B: Surface view of the NMR-derived structural ensemble: The hydrophobic ridge formed in the helical turn by P187, L188, and L191 (dark green) is extended beyond the helical structure by L184 and P185 (light green). This hydrophobic area is flanked by R190 and R192 (blue), H186 (purple) is hardly accessible and Q189 is not accessible from this side (Fig. prepared with PyMol).

conformational ensembles were calculated from assigned signals in NOESY spectra that were converted in distance restraints for structure calculation.

Signals for structure calculation were picked from NOESY spectra 300 ms mixing time. The signal volumes for each residue were converted into distance

	wt α-13-mer				*α-L188A -13-mer*			
Amino acid	*i;i+1*	*i;i+2*	*i;i+3*	*i;i+4*	*i;i+1*	*i;i+2*	*i;i+3*	*i;i+4*
L180	4.0	2.0	-	-	6.5	1.5	-	-
R181	1.5	-	5.0	-	2.5	-	-	-
G182	1.5	1.5	-	-	3.0	2.0	-	-
T183	2.0	-	-	-	2.5	-	-	-
L184	-	2.5	-	-	-	6.5	-	-
P185	-	-	-	-	3.0	-	-	-
H186	-	17.0	**34.0**	**32.5**	-	12.5	13.5	-
P187	-	4.0	**16.5**	**27.0**	-	1.5	-	-
L188/A188	-	2.0	**7.0**	**9.0**	2.0	7.0	-	-
Q189	4.0	-	**1.5**	-	-	-	-	-
R190	2.5	3.0	-	-	9.5	28.5	-	-
L191	4.5	-	-	-	4.5	-	-	-
R192	-	-	-	-	-	-		-

Table 1. Population of hydrogen bonds over a representative 4 ns time span in the MD-simulations with explicit water of the lowest energy NMR structures of the wild-type and the L188A mutant of the ENaC-13-mer peptide. Trajectories were analyzed using the PTRAJ's H-bonding facility giving the average number of inter-residual backbone hydrogen bonds in percent. The table gives the H-bond fractions of the listed residue with those located one (i;i+1), two (i;i+2), three (i;i+3), or four (i;i+4) positions further in the sequence. It can clearly be seen that in the wt peptide residues a significant fraction of H-bonds (numbers printed bold) indicative for helical structures is found between residues 186-189, 186-190, 187-190, and 187-191 and to a much lesser extent between 188-191, 188-189, and 189-192, presumably due to involvement of residues at the fraying terminus of the peptide. These are absent in the L188A mutant indicating a much higher internal flexibility caused by the missing leucine side chain.

restraints following a $1/r^4$ distance dependence after calibration to the intra-residual H^N-H^α signal [42]. Signals were grouped into restraints corresponding to upper distance limits of 3.5, 4.5, and 5.5 Å. It should be noted that – although the NOE-signal intensities and volumes follow a $1/r^6$ dependence [43] – it was empirically found that the $1/r^4$ dependence gives a better distribution of signal intensities, probably caused by effects of internal peptide dynamics.

Overall, a number of structure calculations have been carried out using different subsets of distance restraints. In particular when using all available distance restraints of the wt α-13-mer a significant number of NOE-violations were observed in the resulting structural ensembles. Essentially in all cases problems were found to arise from side chain NOE signals. In small peptides especially the side chains are flexible and can give rise to NOE signals belonging to different conformations, which is a well-known fact [25, 44]. For instance, signals of the imidazole group of H186 were found to simultaneously form contacts with preceding as well as with following residues due to ring flipping events. Hence, only H^α, H^N, and H^β protons were finally used for structure calculation. The resulting structural ensemble exhibits essentially no NOE-violations and resulted in a well converging α-helical conformation in the carboxy-terminal half, while the amino-terminal half is disordered (Fig. 5A). The structures adopt backbone dihedral angles that fall into the allowed regions of the Ramachandran plot. It can clearly be seen that the carboxy-terminus forms helical conformers starting from residue L188 to R192 preceded by a bent structure located at the P185-H186-P187 motif. The helical structure is mainly due to NOE cross peaks between residues H186 and Q189 and Q189 and R192. Importantly, despite evidence for the presence of other conformations, several backbone NOE signals were present that can only exist in helical or turn-like structures. These include cross peak Q189-H^N/L191-H^N and the cross peaks H186-H^α/Q189-H^N, P187- H^α/Q189-H^N, and Q189-H^α/R192-H^N (Fig. 5C). Other NOE signals can be present in helical as well as in elongated conformations. Due to different inter-atomic distances in the respective conformations the NOE-

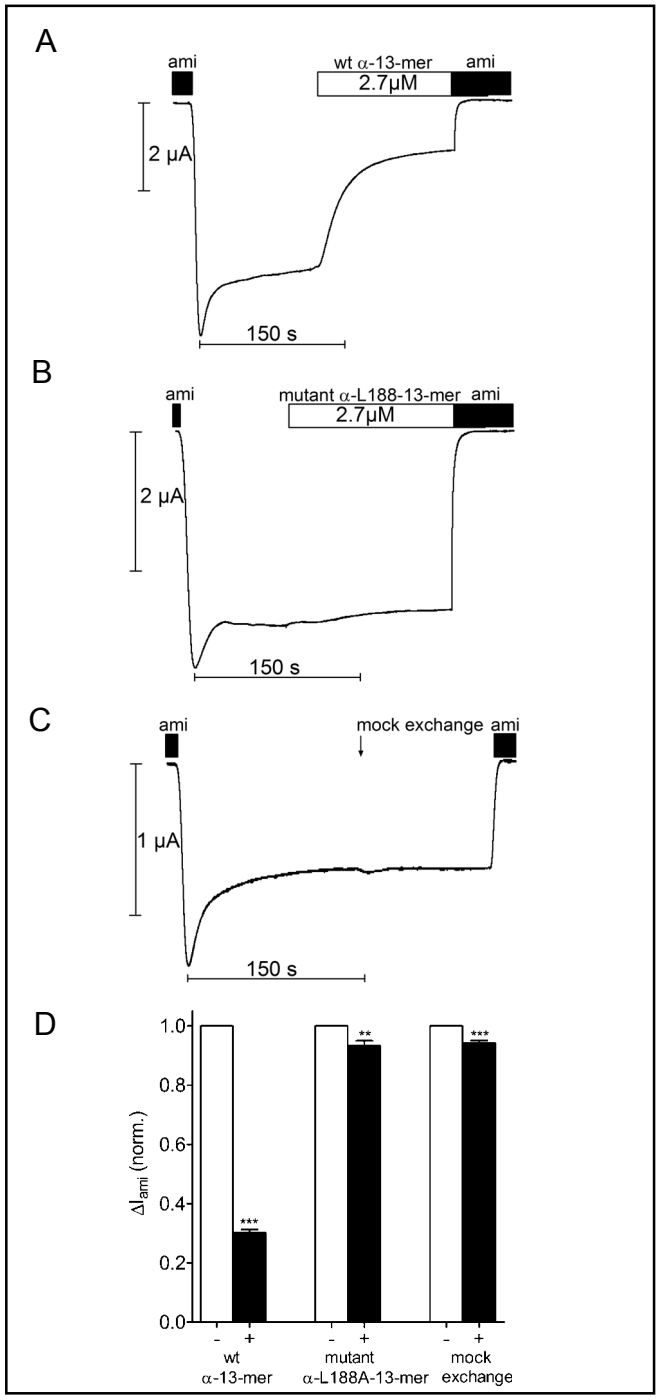

Fig. 7. Comparison of the inhibitory effect of the wt α-13-mer and the mutant α-L188A-13-mer on human ENaC: Current recordings were performed as in figure 1. Representative current traces are shown to illustrate the effects of 2.7 μM wt α-13-mer peptide (A), of 2.7 μM mutant α-L188A-13-mer peptide (B), or of a mock solution exchange in a time matched control experiment (C). Data from similar experiments as shown in A-C are summarized in D as relative change of ΔI_{ami} in response to the wt peptide, the mutant peptide or the mock solution exchange. ΔI_{ami} values were normalized to the corresponding initial ΔI_{ami} value prior to the application of a peptide or the mock solution exchange. **, $p<0.01$; ***, $p<0.001$, paired t-test.

intensities also differ and can be used to evaluate conformational preferences [44]. Such an example is represented by the NOE Q189-H^{α}/R190-H^{N}, which has a slightly weaker intensity than the intra-residual cross peak Q189-H^{α}/H^{N}. The distance for the latter can be assumed to be between 2.8 and 3.0 Å depending on the structure. Hence, a lower intensity indicates a larger inter-atomic distance which argues in favor of a helical conformation, in which this distance would be larger than ~ 4 Å as compared to smaller than ~ 2.5 Å in a β-sheet conformation (Fig. 5C). Similarly, H^{N}-H^{N} NOE-signals between Q189/R190 and R190/L191 indicate helical conformations. The resulting ensemble of preferred conformers shows a helical turn extending from L188 to R192, which is amino-terminally capped by P187. P187 induces a bent turn-like structure rendering H186 to interact with Q189. As a consequence, Q189 appears to be less accessible from the surface while L188 and L191 are fully accessibly for interactions.

In fact, when plotted on a helical wheel the inhibitory sequence forms an amphiphatic helix with a hydrophobic (P187, L188, L191) and a hydrophilic side (Q189, R190, R191) (Fig. 6A). Clustering of the basic residues at the carboxy-terminus could stabilize helical conformations by favorable interactions with the helix dipole. The hydrophobic surface formed by P187, L188, and L191 is amino-terminally extended by the side-chains of P185 and L184 (Fig. 6B). By mutation analysis Carattino et al. [13] showed that essentially all residues in this sequence are required for full inhibitory activity. Only L188 had not been mutated. If the active conformation were helical, an interaction would most likely involve the hydrophobic half of the helix. We hypothesized that changing leucine 188 to alanine, which has a high helix-propensity itself but has a much smaller side chain than leucine, may influence both, the conformational equilibrium and the inhibitory activity of the peptide. To test this hypothesis, an α-L188A-13 mutant peptide was generated, subjected to CD- and NMR-studies, and tested for its inhibitory effect on ENaC currents in the oocyte expression system.

α-L188A-13-mer is also helical although to a lesser content

The mutant peptide also undergoes a coil-to-helix transition upon addition of TFE as judged by CD-spectroscopy (Fig. 3B). However, α-L188A-13-mer displayed a slightly reduced helix content of 23 % as compared to the wt peptide. Again, NMR chemical shift

analysis revealed that the helical structure is located at the carboxy-terminal region of the peptide (Fig. 4). NOESY spectra showed a lower number of inter-residual signals. At 300 ms mixing time only 55 inter-residual NOEs were used for further analysis as compared to 75 in the wt peptide. The resulting ensemble of the 20 lowest energy structures still displays the same turn and helix-like conformations as the wt peptide, although the ensemble is much more heterogeneous (Fig. 5B). The increased conformational diversity results from the reduced number of NOE signals between H186/Q189, Q189/R192, P185/Q189, and H186/L191. This decrease in signals also results in two different capping conformations at P187. In summary, removal of the bulky, hydrophobic side-chain of L188 results in a much less defined backbone and side chain conformations and increased conformational flexibility. Nevertheless, absence of signals of A188 still indicates the presence of conformational exchange. CD-analysis, secondary chemical shifts, and structure calculation identify the presence of residual helicity in the carboxy-terminus of the L188A-mutant, although to a lesser extent than in the wt sequence.

To obtain further insights into the conformational behavior of wt α-13-mer and the mutant α-L188A-13-mer molecular dynamics simulations of the peptides in explicit water were carried out. In particular, we aimed to evaluate whether or not the mutation gives rise to an increased sampling of the conformational space by simulations of the minimum energy conformation of the NMR-ensembles of the two peptides. Evaluating the population of inter-residual H-bonding patterns indeed shows that in the α-13-mer helical structures are significantly populated in the carboxy-terminal half, whereas these are absent in the α-L188A-13-mer peptide (Table 1). Apparently, eliminating the bulky and hydrophobic side chain of leucine eliminates stabilizing side chain contacts and leads to an enhanced sampling of the conformational space.

Comparison of the inhibitory effect of the wt α-13-mer and the mutant α-L188A-13-mer on human ENaC

To investigate whether replacing the leucine 188 by alanine affects the inhibitory action of the 13-mer peptide we compared the effect of the wt α-13-mer with that of the mutant α-L188A-13-mer on ENaC currents in human αβγENaC expressing oocytes. Typical whole-cell current recordings are shown in Fig. 7A-C. Recordings were started in the presence of amiloride and washout of amiloride revealed an ENaC-mediated inward current component. After the ENaC inward current had reached a plateau, the wt 13-mer peptide or the mutant 13-mer peptide was applied. As expected from the results shown in Fig. 1, application of 2.7 μM wt 13-mer peptide (Fig. 7A) caused a significant inhibition of the inward current. In contrast, application of 2.7 μM of mutant peptide had no significant inhibitory effect (Fig. 7B). The small degree of continuous current decline observed in the presence of 2.7 μM of mutant peptide cannot be attributed to a residual inhibitory effect of the mutant peptide since a similar decline was also observed in time matched control experiments with mock solution exchange (Fig. 7C, D). The spontaneous run-down is a well-known characteristic of ENaC currents in the oocyte expression system [39]. Even in a concentration of 27 μM the mutant peptide failed to inhibit ENaC (data not shown). Results from similar experiments as shown in Fig. 7A-C are summarized in Fig. 7D. On average, we observed a 70 ± 1 % reduction of ΔI_{ami} within two minutes of application of the α-13-mer peptide (2.7 μM). In contrast, in the presence of the mutant α-13-mer peptide (2.7 μM) ΔI_{ami} declined only by about 7 ± 2 % within the same time interval. The latter decline was not significantly different from the 6 ± 1 % spontaneous run-down of ΔI_{ami} observed in time matched control experiments. Taken together these results demonstrate that replacing the leucine residue 188 by alanine abolishes the inhibitory effect of the 13-mer peptide on ENaC.

Discussion

In this study, we investigated the structural basis of the inhibitory effect of the human α-13-mer peptide on ENaC. The key findings of our study are the following: 1) Our structural analysis of the α-13-mer peptide indicates that the carboxy-terminus of this peptide forms helical conformers ranging from residue P187 to R192. 2) In functional studies using the *X. laevis* oocyte expression system we demonstrated that replacing the leucine residue 188 by alanine, which should have a strong effect on the conformational preference of the α-13-mer peptide, abolishes its inhibitory effect on human ENaC.

A previous analysis of the mouse α-8-mer peptide performed by solution-state NMR spectroscopy provided no evidence of secondary or tertiary structure, suggesting that the peptide has a random coil conformation in aqueous solution. However, detailed structure-activity

studies indicated that a characteristic PHP motif within the α-8-mer peptide is essential for the peptide's inhibitory effect on ENaC [13]. In the present study, we used a homologous human α-13-mer peptide that was amino-terminally extended to enhance its solubility. Initial 1D-NMR experiments indicated that the α-13 variant of the inhibitory ENaC peptide shows an unexpected low number of resonances, which was attributed to chemical exchange. This behavior apparently was not observed with the mouse α-8-mer peptide [13] and is likely to be caused by the amino-terminal extension of the human α-13-mer peptide which places the PHP motif in the center of the peptide instead of being at the amino-terminus in the α-8-mer peptide. The conformational exchange observed in our peptide prompted us to explore whether or not preferred conformers can be found for this peptide by computational methods. Indeed, we found that the carboxy-terminal part of the α-13-mer peptide has a tendency to populate helical conformers. The intrinsic helix propensity of this sequence could be confirmed in CD studies by addition of the helix-promoting agent TFE. We used TFE to shift the equilibrium of inter-converting conformations in the inhibitory ENaC α-13-mer peptide towards helical conformers, which we assume to be stabilized by tertiary interactions upon binding to the fully assembled ENaC channel.

In fact, utilizing CD- and 2D-NMR-spectroscopy we were able to corroborate the presence of helical conformations in the inhibitory ENaC α-13-mer peptide. Critical evaluation of the NMR-data reveals that the carboxy-terminal half of the peptide forms a helical turn being capped by the PHP motif, while the amino-terminal part of the peptide is flexible. In this context it is important to emphasize that in small peptide systems, such as the wt α-13-mer, it is highly unlikely to obtain a single, rigid 3D-conformer in the sense of a well-defined and rigid protein structure. This is largely due to the lower number of stabilizing contacts that can be established. Rather, one looks at an ensemble of interchanging conformations. In certain cases, one conformation may prevail or be energetically preferred over others. In such cases it is often found that such a preferred conformation also exhibits biological activity and, e.g., is selected through a binding event. This is known as induced fit or, more general, conformational selection [45-47]. However, by combining experimental and computational approaches it is possible to address the conformational properties of peptides exhibiting residual structure [44]. In this study, the population of a preferred conformer is increased by application of a co-solvent and both, experiment and theory indicate that – averaged over time – helical conformations prevail in the carboxy-terminal half covering most of the inhibitory active sequence. Nevertheless, we wish to emphasize that the conformers obtained – although being the most abundant one – are part of a dynamic ensemble of peptide conformations in solution. In fact, some NOE signals were found to be incompatible with the preferred conformations as a result of conformational averaging. Conformational exchange is further evidenced by the fact that 2D-NMR spectra for structure evaluation could only be recorded at a lowered temperature. Despite optimization of the temperature we still observe broadening of NMR signals indicative for conformational exchange in particular at residue L/A188, which is adjacent to the PHP motif capping the carboxy-terminal helical turn and which may point towards a possible cis-trans isomerisation at P187.

Carattino et al. [13] conducted an extensive mutation study (without including position L188) to identify residues that are important for the inhibitory activity of the ENaC α-8-mer. If the α-13-mer was active in a helical conformation, a decrease in its inhibitory activity would be expected upon mutation of leucine 188. Indeed, using electrophysiological experiments we demonstrated that a change of leucine 188 to alanine in the 13-mer peptide abolished its inhibitory activity on ENaC.

Recent findings of Kashlan et al. indicate that the α-8-mer is an allosteric regulator of ENaC activity [18]. By mutating several residues in ENaC and in the α-8-mer peptide simultaneously, Kashlan and colleagues were able to determine putative contacts between residues H186 and L191 within the α-8-mer peptide and ENaC. Moreover, based on sequence comparisons of ENaC and XC6422 from *Xanthomonas campestris* (PDB code 2FUK), they also predict an α-helical conformation for the sequence investigated here. Although these findings in general corroborate the results presented here, it should be noted that according to the model proposed by Kashlan et al. the entire sequence corresponding to the α-13-mer forms one continuous α-helix of three turns length. As a result, the PHP sequence would come to reside in the center of the helix, which most likely results in a strong kink or even the termination of the helix as observed in our structures. Hence, our data provide experimental evidence for the presence of helical conformations in the allosteric inhibitory sequence. In particular, we show that helical conformations are confined to the carboxy-terminal

part, where P187, L188, and L191 form a surface accessible hydrophobic ridge that is amino-terminally extended by L184 and P185. In our structural model this putative hydrophobic interaction surface is flanked by the positive charges of R190 and R192, respectively. Neither H186 – which is largely inaccessible – nor Q187 – which is completely inaccessible from this side of the helical turn – seem to play an important role for the interaction. In this context it is interesting to note that Carattino et al. [13] found in a mutational study of the corresponding peptide derived from mouse ENaC that the inhibitory function is not reduced when the residues corresponding to L184 or L191 are mutated to large, hydrophobic groups [13]. Mutation to alanine or asparagine abolishes ENaC inhibition. Similarly, removing the two prolines or mutation of the histidine embedded by these prolines to glutamate or lysine significantly reduces the inhibitory activity of the peptide. By contrast, mutation of the histidine to tyrosine leaves the inhibitory activity essentially unchanged, indicating that not the positive charge but the steric properties of the side chain appear to be critical at this position. Overall, it appears that the PHP motif is optimized for rigidity and to properly orient the preceding leucine. The role of residue L188 has not been investigated before, but as shown in this study, reduction of the hydrophobic surface also leads to reduction of inhibitory activity. The positive charge of R190 seems to be beneficial, but not crucial for action, as mutation to lysine slightly reduces activity, but mutation to alanine or even glutamate is not suited to abolish the inhibitory activity of the peptide. Mutational and structural data therefore allow proposing functions to the individual amino acids of the inhibitory active peptide [13].

In this context it is an interesting observation that mutation of essentially every position of the α-8-mer peptide affects its inhibitory activity. There are two possible explanations for this behavior. First, one could envision binding in a conformation where all residues of the α-8-mer are in contact with the extracellular region of ENaC that is critically important for mediating the structural change of the channel during proteolytic channel activation. This could in principle be achieved by binding in an elongated conformation. However, this would also require a rather large binding interface reminiscent of the epitope-recognizing interface of antibodies [48, 49]. Another possibility is that the binding occurs in a defined conformation – such as the one described here – where mutations either affect residues directly interacting with ENaC or simply interfere with the conformation required for binding. This scenario for an allosteric regulation of ENaC by the α-8-mer-/α-13-mer peptides would be in good agreement with recent mutational studies as well as with the structural data presented in this study.

At present it is not possible to establish a final mechanism, as it is not known whether or not L188 is involved in the molecular interface with ENaC. Assuming that the α-13-mer is active in an α-helical conformation, L188 could indeed form contacts with ENaC as part of the hydrophobic surface formed in the helix. In this case mutation to alanine would diminish many *Van-der-Waals* interactions leading to a reduced inhibitory activity. However, NMR and CD experiments as well as computational studies both show that this mutation also affects the conformational and dynamical properties of the α-13-mer peptide thereby also modulating its activity. In fact, a complex interplay of diverse effects may be involved in the allosteric regulation of ENaC activity by the α-13-mer peptide. To precisely determine where and how the αENaC peptide exerts its inhibitory activity on the extracellular domain of ENaC, high resolution structural information on the complex of the inhibitory αENaC peptide with cleaved and uncleaved ENaC are needed.

Acknowledgements

The authors thank Prabhu S. Thirupahti for recording CD-spectra of the wt α-13-mer. Furthermore, the expert technical assistance of Ralf Rinke is gratefully acknowledged.

This study was supported by grants of the Deutsche Forschungsgemeinschaft (SFB423: Kidney injury: Pathogenesis and Regenerative Mechanisms; project A12; C.K.), the Johannes and Frieda Marohn Stiftung (C.K.), an Elite Network of Bavaria (ENB) fellowship (S.H.), the BioMedTec International Graduate School (BIGSS) 'Lead Structures of Cell Function' of the ENB (S.H., D.S.), a young investigator grant from the IZKF (Interdisciplinary Centre of Clinical Research) (S.H.), and the ELAN program of the Friedrich-Alexander-Universität Erlangen-Nürnberg (S.H.).

References

1 Kellenberger S, Schild L: Epithelial sodium channel/degenerin family of ion channels: A variety of functions for a shared structure. Physiol Rev 2002;82:735-767.

2 Rossier BC, Schild L: Epithelial sodium channel: Mendelian versus essential hypertension. Hypertension 2008;52:595-600.

3 Loffing J, Korbmacher C: Regulated sodium transport in the renal connecting tubule (CNT) via the epithelial sodium channel (ENaC). Pflügers Arch 2009;458:111-135.

4 Canessa CM: Structural biology: Unexpected opening. Nature 2007;449:293-294.

5 Jasti J, Furukawa H, Gonzales EB, Gouaux E: Structure of acid-sensing ion channel 1 at 1.9 a resolution and low pH. Nature 2007;449:316-323.

6 Stockand JD, Staruschenko A, Pochynyuk O, Booth RE, Silverthorn DU: Insight toward epithelial Na^+ channel mechanism revealed by the acid-sensing ion channel 1 structure. IUBMB Life 2008;60:620-628.

7 Stewart AP, Haerteis S, Diakov A, Korbmacher C, Edwardson JM: Atomic force microscopy reveals the architecture of the epithelial sodium channel (ENaC). J Biol Chem 2011;286:31944-31952.

8 Kleyman TR, Carattino MD, Hughey RP: ENaC at the cutting edge: Regulation of epithelial sodium channels by proteases. J Biol Chem 2009;284:20447-20451.

9 Rossier BC, Stutts MJ: Activation of the epithelial sodium channel (ENaC) by serine proteases. Annu Rev Physiol 2009;71:361-379.

10 Hughey RP, Bruns JB, Kinlough CL, Kleyman TR: Distinct pools of epithelial sodium channels are expressed at the plasma membrane. J Biol Chem 2004;279:48491-48494.

11 Carattino MD, Sheng S, Bruns JB, Pilewski JM, Hughey RP, Kleyman TR: The epithelial Na^+ channel is inhibited by a peptide derived from proteolytic processing of its alpha subunit. J Biol Chem 2006;281:18901-18907.

12 Bruns JB, Carattino MD, Sheng S, Maarouf AB, Weisz OA, Pilewski JM, Hughey RP, Kleyman TR: Epithelial Na^+ channels are fully activated by furin- and prostasin-dependent release of an inhibitory peptide from the gamma subunit. J Biol Chem 2007;282:6153-6160.

13 Carattino MD, Passero CJ, Steren CA, Maarouf AB, Pilewski JM, Myerburg MM, Hughey RP, Kleyman TR: Defining an inhibitory domain in the alpha-subunit of the epithelial sodium channel. Am J Physiol Renal Physiol 2008;294:F47-52.

14 Passero CJ, Carattino MD, Kashlan OB, Myerburg MM, Hughey RP, Kleyman TR: Defining an inhibitory domain in the gamma subunit of the epithelial sodium channel. Am J Physiol Renal Physiol 2010;299:F854-861.

15 Knight KK, Olson DR, Zhou R, Snyder PM: Liddle's syndrome mutations increase Na^+ transport through dual effects on epithelial Na^+ channel surface expression and proteolytic cleavage. Proc Natl Acad Sci USA 2006;103:2805-2808.

16 Haerteis S, Krueger B, Korbmacher C, Rauh R: The delta-subunit of the epithelial sodium channel (ENaC) enhances channel activity and alters proteolytic ENaC activation. J Biol Chem 2009;284:29024-29040.

17 Hu JC, Bengrine A, Lis A, Awayda MS: Alternative mechanism of activation of the epithelial Na^+ channel by cleavage. J Biol Chem 2009;284:36334-36345.

18 Kashlan OB, Boyd CR, Argyropoulos C, Okumura S, Hughey RP, Grabe M, Kleyman TR: Allosteric inhibition of the epithelial Na^+ channel through peptide binding at peripheral finger and thumb domains. J Biol Chem 2010;285:35216-35223.

19 Kashlan OB, Adelman JL, Okumura S, Blobner BM, Zuzek Z, Hughey RP, Kleyman TR, Grabe M: Constraint-based, homology model of the extracellular domain of the epithelial Na^+ channel alpha subunit reveals a mechanism of channel activation by proteases. J Biol Chem 2011;286:649-660.

20 Rauh R, Diakov A, Tzschoppe A, Korbmacher J, Azad AK, Cuppens H, Cassiman JJ, Dotsch J, Sticht H, Korbmacher C: A mutation of the epithelial sodium channel associated with atypical cystic fibrosis increases channel open probability and reduces Na^+ self inhibition. J Physiol 2010;588:1211-1225.

21 Case DA, Darden TA, Cheatham TE, III, Simmerling CL, Wang J, Duke RE, Luo R, Crowley M, Walker RC, Zhang W, Merz KM, Wang B, Hayik S, Roitberg A, Seabra G, Kolossváry I, Wong KF, Paesani F, Vanicek J, Wu X, Brozell SR, Steinbrecher T, Gohlke H, Yang L, Tan C, Mongan J, Hornak V, Cui G, Mathews DH, Seetin MG, Sagui C, Babin V, Kollman PA: AMBER 10, University of California, San Francisco, 2008.

22 Scopes RK: Measurement of protein by spectrophotometry at 205 nm. Anal Biochem 1974;59:277-282.

23 Stoscheck CM: Quantitation of protein. Methods Enzymol 1990;182:50-68.

24 Chen YH, Yang JT, Chau KH: Determination of the helix and beta form of proteins in aqueous solution by circular dichroism. Biochemistry 1974;13:3350-3359.

25 Wüthrich K: NMR of proteins and nucleic acids. Wiley, New York 1986.

26 Delaglio F, Grzesiek S, Vuister GW, Zhu G, Pfeifer J, Bax A: NMRpipe: A multidimensional spectral processing system based on unix pipes. J Biomol NMR 1995;6:277-293.

27 Johnson BA, Blevins RA: NMRview: A computer program for the visualization and analysis of NMR data. J Biomol NMR 1994;4:603-614.

28 Wishart DS, Sykes BD, Richards FM: Relationship between nuclear magnetic resonance chemical shift and protein secondary structure. J Mol Biol 1991;222:311-333.

29 Schwarzinger S, Kroon GJ, Foss TR, Wright PE, Dyson HJ: Random coil chemical shifts in acidic 8 m urea: Implementation of random coil shift data in NMRview. J Biomol NMR 2000;18:43-48.

30 Schwarzinger S, Kroon GJ, Foss TR, Chung J, Wright PE, Dyson HJ: Sequence-dependent correction of random coil NMR chemical shifts. J Am Chem Soc 2001;123:2970-2978.

31 Brunger AT, Nilges M: Computational challenges for macromolecular structure determination by x-ray crystallography and solution NMR-spectroscopy. Q Rev Biophys 1993;26:49-125.

32 Schwieters CD, Kuszewski JJ, Tjandra N, Clore GM: The xplor-nih NMR molecular structure determination package. J Magn Reson 2003;160:65-73.

33 Schwieters CD, Kuszewski JJ, Clore GM: Using xplor-nih for NMR molecular structure determination. Progr NMR Spectroscopy 2006;48:47-62.

34 Laskowski RA, Rullmannn JA, MacArthur MW, Kaptein R, Thornton JM: Aqua and procheck-NMR: Programs for checking the quality of protein structures solved by NMR. J Biomol NMR 1996;8:477-486.

35 Humphrey W, Dalke A, Schulten K: Vmd: Visual molecular dynamics. J Mol Graph 1996;14:33-38, 27-38.

36 Hornak V, Abel R, Okur A, Strockbine B, Roitberg A, Simmerling C: Comparison of multiple amber force fields and development of improved protein backbone parameters. Proteins 2006;65:712-725.

37 Chraibi A, Horisberger JD: Na^+ self inhibition of human epithelial Na^+ channel: Temperature dependence and effect of extracellular proteases. J Gen Physiol 2002;120:133-145.

38 Huber R, Krueger B, Diakov A, Korbmacher J, Haerteis S, Einsiedel J, Gmeiner P, Azad AK, Cuppens H, Cassiman JJ, Korbmacher C, Rauh R: Functional characterization of a partial loss-of-function mutation of the epithelial sodium channel (ENaC) associated with atypical cystic fibrosis. Cell Physiol Biochem 2010;25:145-158.

39 Volk T, Konstas AA, Bassalay P, Ehmke H, Korbmacher C: Extracellular Na^+ removal attenuates rundown of the epithelial Na^+-channel (ENaC) by reducing the rate of channel retrieval. Pflügers Arch 2004;447:884-894.

40 Buck M: Trifluoroethanol and colleagues: Cosolvents come of age. Recent studies with peptides and proteins. Q Rev Biophys 1998;31:297-355.

41 Reymond MT, Merutka G, Dyson HJ, Wright PE: Folding propensities of peptide fragments of myoglobin. Protein Sci 1997;6:706-716.

42 Güntert P, Braun W, Wüthrich K: Efficient computation of three-dimensional protein structures in solution from nuclear magnetic resonance data using the program diana and the supporting programs caliba, habas and glomsa. J Mol Biol 1991;217:517-530.

43 Neuhaus D, Williamson MP: The NOE in structural and conformational analysis. Wiley, New York 1989.

44 Camilloni C, Schaal D, Schweimer K, Schwarzinger S, De Simone A: Energy landscape of the prion protein helix 1 probed by metadynamics and NMR. Biophys J 2012;102:158-167.

45 Demarest SJ, Martinez-Yamout M, Chung J, Chen H, Xu W, Dyson HJ, Evans RM, Wright PE: Mutual synergistic folding in recruitment of cbp/p300 by p160 nuclear receptor coactivators. Nature 2002;415:549-553.

46 Boehr DD, Nussinov R, Wright PE: The role of dynamic conformational ensembles in biomolecular recognition. Nat Chem Biol 2009;5:789-796.

47 Csermely P, Palotai R, Nussinov R: Induced fit, conformational selection and independent dynamic segments: An extended view of binding events. Trends Biochem Sci 2010;35:539-546.

48 Sundberg EJ: Structural basis of antibody-antigen interactions. Methods Mol Biol 2009;524:23-36.

49 Mangels C, Kellner R, Einsiedel J, Weiglmeier PR, Rösch P, Gmeiner P, Schwarzinger S: The therapeutically anti-prion active antibody-fragment scfv-w226: Paramagnetic relaxation-enhanced NMR spectroscopy aided structure elucidation of the paratope-epitope interface. J Biomol Struct Dyn 2010;28:13-22.